INTERNATIONAL JOURNAL OF ROBUST AND NONLINEAR CONTROL
Int. J. Robust Nonlinear Control 2002; **12**:869–896 (DOI: 10.1002/rnc.708)

Control of a thrust-vectored flying wing: a receding horizon—LPV approach

Ali Jadbabaie[1,*,†] and John Hauser[2]

[1] *Department of Electrical Engineering, Yale University, New Haven, CT 06520, U.S.A.*
[2] *Electrical and Computer Engineering and Aerospace Engineering, University of Colorado, Boulder, CO 80309-0425, U.S.A.*

SUMMARY

This paper deals with the application of receding horizon methods to hover and forward flight models of an experimental tethered flying wing developed at Caltech. The dynamics of the system are representative of a vertical landing and take off aircraft, such as a Harrier around hover, or a thrust-vectored aircraft such as F18-HARV or X-31 in forward flight. The adopted control methodology is a hybrid of receding horizon techniques and control Lyapunov function (CLF)-based ideas.

First, a CLF is generated using quasi-LPV methods and then, by using the CLF as the terminal cost in the receding horizon optimization, stability is guaranteed. The main advantage of this approach is that stability can be guaranteed without imposing constraints in the on-line optimization, allowing the problem to be solved in a more efficient manner. Models of the experimental set-up are obtained for the hover and forward flight modes. Numerical simulations for different time horizons are presented to illustrate the effectiveness of the discussed methods. Specifically, it is shown that a mere upper bound on the cost-to-go is not an appropriate choice for a terminal cost, when the horizon length is short. Simulation results are presented using experimentally verified model parameters.

1. INTRODUCTION

In receding horizon control, an open-loop finite horizon optimization is solved. The resulting open-loop control trajectory is applied to the system for a fraction of the horizon length. This process is then repeated, resulting in a sampled feedback law. Although receding horizon control has been successfully used in the process control industry, its application to stability critical areas has been more difficult. This is mainly due to two reasons. The first problem stems from the fact that the finite horizon optimizations have to be solved in a relatively short period of time. Second, it is well known and can be easily demonstrated using linear examples that a

*Correspondence to: Ali Jadbabaie, Department of Electrical Engineering, Yale University, New Haven, CT 06520, U.S.A.
† E-mail: ali.jadbabaie@yale.edu

Contract/grant sponsor: AFOSR
Contract/grant sponsor: DARPA

naive application of the receding horizon strategy can have disastrous effects and renders the system unstable. Several different approaches have been proposed to tackle this problem. (See Reference [1] for an excellent review of this literature.)

These approaches used additional end-point equality constraints [2] or end-point inequality constraints [3–7], in order to guarantee closed-loop stability. An alternative approach was presented in Reference [8], where the authors use an *a priori* obtained control Lyapunov function (CLF) to guarantee stability. In this approach, stability is *enforced* by imposing additional constraints requiring that the derivative of the CLF along the optimal trajectory be negative definite and that the decrease in the value of the CLF at the end of the horizon be larger along the optimal trajectory than the CLF trajectory. This approach assumes the existence of a global control Lyapunov function.

Recently, another approach was developed by the authors in Reference [9]. Similar to Reference [8], this approach obtained stability guarantees through the use of an *a priori* obtained CLF. However, the CLF was used as terminal cost. By utilizing a suitable control Lyapunov function, the stability of the receding horizon scheme is guaranteed in a more efficient manner. In this setting, it was shown that the stability constraints are automatically satisfied, and can be eliminated from the optimization. This resulted in a speedup in the computations.

Furthermore, it was shown in Reference [9] that the region of attraction of the unconstrained receding horizon control law is always larger than that of the CLF and it can be grown further to contain any compact subset of the infinite horizon region of attraction by a suitable choice of the horizon length.

The purpose of this paper is to demonstrate the use of a stabilizing receding horizon strategy on hover and forward flight models of the Caltech-ducted fan. Although we only discuss simulation results in this paper, it should be noted that the model parameters were developed using actual flight experiments.

This paper is organized as follows: in Section 2, we formulate the problem and present our notation. Section 3 is a review of the unconstrained receding horizon scheme with a CLF terminal cost [10,11]. The quasi-LPV approach for obtaining a CLF is discussed in Section 4. Details of the Caltech-ducted fan experiment are discussed in Section 5, where the models of the experiment at hover and forward flight are discussed in addition to simulation results. Finally, our conclusions are presented in Section 6.

2. PROBLEM SETTING

The nonlinear system under consideration is

$$\dot{x} = f(x, u)$$

where the vector field $f : \mathbb{R}^n \times \mathbb{R}^m \to \mathbb{R}^n$ is C^2 and possesses a linearly controllable critical point at the origin, e.g. $f(0,0) = 0$ and $(A, B) := (D_1 f(0,0), D_2 f(0,0))$ is controllable. Given an initial state x and a control trajectory $u(\cdot)$, the state trajectory $x^u(\cdot\,; x)$ is the (absolutely continuous) curve in $\mathbb{R}^n$ satisfying

$$x^u(t; x) = x + \int_0^t f(x^u(\tau; x), u(\tau))\, \mathrm{d}\tau$$

for $t \geqslant 0$.

The performance of the system will be measured by a given incremental cost $q : \mathbb{R}^n \times \mathbb{R}^m \to \mathbb{R}$ that is C^2 and fully penalizes both state and control according to

$$q(x,u) \geqslant c_q(\|x\|^2 + \|u\|^2), \quad x \in \mathbb{R}^n, \ \ u \in \mathbb{R}^m$$

for some $c_q > 0$ and $q(0,0) = 0$. It follows that the quadratic approximation of q at the origin is positive definite, $D^2q(0,0) \geqslant c_q I > 0$.

To ensure that the solutions of the optimization problems of interest are nice, we impose some convexity conditions. We require the set $f(x,\mathbb{R}^m) \subset \mathbb{R}^n$ to be convex for each $x \in \mathbb{R}^n$. We also require that the pre-Hamiltonion function $u \mapsto p^{\mathrm{T}} f(x,u) + q(x,u) =: K(x,u,p)$ be strictly convex for each $(x,p) \in \mathbb{R}^n \times \mathbb{R}^n$ and that there is a C^2 function $\bar{\boldsymbol{u}}^* : \mathbb{R}^n \times \mathbb{R}^n \to \mathbb{R}^m : (x,p) \mapsto \bar{\boldsymbol{u}}^*(x,p)$ providing the global minimum of $K(x,u,p)$. These conditions are trivially satisfied for control affine f and quadratic q.

The cost of applying a control $u(\cdot)$ from an initial state x over the infinite time interval $[0,\infty)$ is given by

$$J_\infty(x,u(\cdot)) = \int_0^\infty q(x^u(\tau;x),u(\tau))\,\mathrm{d}\tau$$

The optimal cost (from x) is given by

$$J_\infty^*(x) = \inf_{u(\cdot)} J_\infty(x,u(\cdot))$$

where the control functions $u(\cdot)$ belong to some reasonable class of admissible controls (e.g. piecewise continuous or measurable). The function $x \mapsto J_\infty^*(x)$ is often called the *optimal value function* for the infinite horizon optimal control problem.

For practical purposes, we are interested in finite horizon approximations of the infinite horizon optimization problem. In particular, let $V(\cdot)$ be a non-negative C^2 function with $V(0) = 0$ and define the finite horizon cost (from x using $u(\cdot)$) to be

$$J_T(x,u(\cdot)) = \int_0^{\mathrm{T}} q(x^u(\tau;x),u(\tau))\,\mathrm{d}\tau + V(x^u(T;x))$$

and denote the optimal cost (from x) as

$$J_T^*(x) = \inf_{u(\cdot)} J_T(x,u(\cdot))$$

As in the infinite horizon case, one can show, by geometric means, that $J_T^*(\cdot)$ is locally smooth (C^2). Other properties will depend on the choice of V and T.

Let Γ^∞ denote the domain of $J_\infty^*(\cdot)$ (the subset of $\mathbb{R}^n$ on which J_∞^* is finite). It is not too difficult to show that the cost functions $J_\infty^*(\cdot)$ and $J_T^*(\cdot)$, $T \geqslant 0$, are continuous functions on Γ_∞ using the same arguments as in Proposition 3.1 of Reference [12]. For simplicity, we will allow $J_\infty^*(\cdot)$ to take values in the extended real line so that, for instance, $J_\infty^*(x) = +\infty$ means that there is no control taking x to the origin.

The infinite horizon cost $J_\infty^*(\cdot)$ is proper on its domain so that the sublevel sets

$$\Gamma_r^\infty \coloneqq \{x \in \Gamma^\infty : J_\infty^*(x) \leqslant r^2\}$$

are compact and path connected and moreover $\Gamma^\infty = \bigcup_{r\geqslant 0} \Gamma_r^\infty$. We refer to sublevel sets of $J_T^*(\cdot)$ and $V(\cdot)$ using

$\Gamma_r^{\mathrm{T}} \coloneqq$ path connected component of $\{x \in \Gamma^\infty\colon J_T^*(x) \leqslant r^2\}$ containing 0 and
$\Omega_r \coloneqq$ path connected component of $\{x \in \mathbb{R}^n\colon V(x) \leqslant r^2\}$ containing 0

3. UNCONSTRAINED RECEDING HORIZON CONTROL WITH CLF TERMINAL COST

Receding horizon control provides a practical strategy for the use of model information through on-line optimization. Every δ seconds, an optimal control problem is solved over a T second horizon, starting from the current state. The first δ seconds of the optimal control $u_T^*(\cdot\,; x(t))$ is then applied to the system, driving the system from $x(t)$ at current time t to $x_T^*(\delta, x(t))$ at the next sample time $t+\delta$. We denote this receding horizon scheme as $\mathscr{RH}(T,\delta)$.

In defining (unconstrained) finite horizon approximations to the infinite horizon problem, the key design parameters are the terminal cost function $V(\cdot)$ and the horizon length T (and, perhaps also, the increment δ).

It is well known (and easily demonstrated with linear examples), that simple truncation of the integral (i.e. $V(x) \equiv 0$) may have disastrous effects if $T > 0$ is too small. Indeed, although the resulting value function may be nicely behaved, the 'optimal' receding horizon closed-loop system can be unstable.

A more considered approach is to make good use of a suitable terminal cost $V(\cdot)$. Evidently, the best choice for the terminal cost is $V(x) = J_\infty^*(x)$ since then the optimal finite and infinite horizon costs are the same. Of course, if *the* optimal value function were available there would be no need to solve a trajectory optimization problem. What properties of the optimal value function should be retained in the terminal cost? To be effective, the terminal cost should account for the discarded tail by ensuring that the origin can be reached from the terminal state $x^u(T;x)$ in an efficient manner (as measured by q). One way to do this is to use an appropriate CLF which is also an upper bound on the cost-to-go.

The following theorem shows that the use of a particular type of CLF is in fact effective, providing rather strong and specific guarantees.

Theorem 1 (Jadbabaie *et al.* [9], Mayne *et al.* [1])
Suppose that the terminal cost $V(\cdot)$ is a control Lyapunov function such that

$$\min_{u\in\mathbb{R}^m} (\dot{V} + q)(x,u) \leqslant 0, \quad x \in \Omega_{r_v} \tag{1}$$

for some $r_v > 0$. Then, for *every* $T > 0$ and $\delta \in (0, T]$, the receding horizon scheme $\mathscr{RH}(T,\delta)$ is exponentially stabilizing. For each $T > 0$, there is an $\bar{r}(T) \geqslant r_v$ such that $\Gamma_{\bar{r}(T)}^{\mathrm{T}}$ is contained in the region of attraction of $\mathscr{RH}(T,\delta)$. Moreover, given any compact subset Λ of Γ^∞, there is a T^* such that $\Lambda \subset \Gamma_{\bar{r}(T)}^{\mathrm{T}}$ for all $T \geqslant T^*$.

Theorem 1 shows that for *any* horizon length $T > 0$ and *any* sampling time $\delta \in (0, T]$, the receding horizon scheme is exponentially stabilizing over the set $\Gamma_{r_v}^{\mathrm{T}}$. For a given T, the region of attraction estimate is enlarged by increasing r beyond r_v to $\bar{r}(T)$ according to the requirement that $V(x_T^*(T;x)) \leqslant r_v^2$ on that set. An important feature of the above result is that, for operations

with the set $\Gamma^{\mathrm{T}}_{\tilde{r}(T)}$, there is no need to impose stability ensuring constraints which would likely make the on-line optimizations more difficult and time consuming to solve. Of course, this method requires a suitable CLF. In the next section, we review a technique known as quasi-linear parameter varying (quasi-LPV) method, which allows us to construct a suitable CLF for the receding horizon strategy described above.

4. QUASI-LPV METHODS

The purpose of this section is to utilize a quasi-LPV methodology to obtain a CLF satisfying (1). This approach was originally developed to design controllers for linear systems with *time varying parameters*, hence the terminology linear parameter varying (LPV) control [13]. The varying parameter $\rho(t)$ is assumed to be available for measurement in real time. Moreover, it is assumed that the parameter trajectories $\rho(\cdot)$ evolve in a compact set, with possible constraints on the rate of variation. Although these conditions limit the application of this strategy, it has been successfully used in the aerospace industry.

A variant of this approach, known as the *quasi*-LPV strategy, can be used to design controllers for certain *nonlinear* systems. The main ideas are much the same, except for the fact that the varying parameters are a function of the states. The so-called quasi-LPV representation of an input-affine nonlinear system has the form

$$\dot{x} = A(\rho(x))x + B(\rho(x))u \tag{2}$$

where the desired trajectory is $x(t) \equiv 0$. We will assume that the *parameter* trajectory $\rho(x(t))$ belongs to a compact set $\mathscr{P} \subset \mathbb{R}^m$ with variations limited according to

$$\underline{v}_i \leqslant \frac{\mathrm{d}}{\mathrm{d}t}\rho_i(x(t)) \leqslant \bar{v}_i, \quad i = 1, \ldots, p \tag{3}$$

for all t. Generalizing the linear quadratic regulator, we are interested in finding a control that makes the cost

$$\int_0^\infty x(\tau)^{\mathrm{T}} Q(\rho(x(\tau)))x(\tau) + u(\tau)R(\rho(x(\tau)))u(\tau)\,\mathrm{d}\tau \tag{4}$$

small. As in the LQR case, one may be able to use linear matrix inequalities (LMIs) to construct a feedback control. Indeed, if there is a positive definite matrix $X(\rho)$ such that

$$\begin{bmatrix} -\sum_{i=1}^{p} \underline{\bar{v}}_i \dfrac{\partial X}{\partial \rho_i}(\rho) + A(\rho)X(\rho) + X(\rho)A(\rho)^{\mathrm{T}} - B(\rho)R(\rho)^{-1}B(\rho)^{\mathrm{T}} & X(\rho)C(\rho)^{\mathrm{T}} \\ C(\rho)X(\rho) & -I \end{bmatrix} < 0 \tag{5}$$

for all $\rho \in \mathscr{P}$ where $C(\rho) = Q(\rho)^{1/2}$, then the closed-loop system with the state feedback

$$u(x) = -R(\rho(x))^{-1}B(\rho(x))^{\mathrm{T}}X(\rho(x))^{-1}x$$

is stable provided that the variation limits (3) are satisfied. Moreover, an upper bound (which also serves as a CLF) on the resulting cost (4) is given by

$$V(x) = x^{\mathrm{T}}X(\rho(x))^{-1}x$$

This upper bound can be minimized (searching over $X(\cdot)$) with the help of a suitable slack variable. Note also, that the CLF $V(\cdot)$ automatically satisfies (1), since the above feedback minimizes $(\dot{V}+q)(x,u)$.

The notation $\sum_{i=1}^{p}\bar{\underline{\nu}}_i$ above means that every combination of $\bar{\nu}_i$ and $\underline{\nu}_i$ should be included in the inequality. For instance, when $p=2, \bar{\nu}_1+\bar{\nu}_2$, $\bar{\nu}_1+\underline{\nu}_2$, $\underline{\nu}_1+\bar{\nu}_2$ and $\underline{\nu}_1+\underline{\nu}_2$ should be $\nu_1$checked individually. In other words, (5) actually represents 2^p inequalities. Additionally, solving (5) involves gridding the parameter space $\mathscr{P}$ and choosing a finite set of basis functions for $X(\rho)$ (see Reference [14] for details). As can be easily seen, the number of LMIs grows exponentially with the number of varying parameters. Furthermore, the gridding technique can be quite costly. Due to these restrictions this method is usually suitable when there are only a few varying parameters (states) in the state-dependent representation.

The quasi-LPV procedure can be simplified, if the search is limited to quadratic Lyapunov functions instead of parameter-dependent Lyapunov functions. In this case, there is no need to have *a priori* bounds on the parameter variations and the 2^p inequalities in (5) reduces to a single matrix inequality for each gridding point. This simplicity comes at the expense of potential conservatism.

From a theoretical point of view, in order to guarantee stability, gridding has to be finer than a critical limit [14]. However, finding this limit requires knowledge of some information about the nonlinear system (e.g. Lipschitz constants) that is not readily available. Also, the level of gridding indicated is likely to be quite conservative making such an approach somewhat impractical. Hence, gridding remains an *ad hoc* procedure.

Moreover, the non-uniqueness of the state-dependent representation of a nonlinear system can make the results conservative. This issue of the state-dependent representation can be addressed by including an additional degree of freedom in the optimization [15,16].

Nevertheless, due to the fact that bounds on the parameter variations are taken into account, stability arguments are more powerful than regular gain scheduling or the state-dependent Ricatti equation method [17]. The quasi-LPV control techniques have been successfully employed in a variety of aerospace applications [18].

In the next section, we outline the use of the CLF obtained from LPV methods in the receding horizon strategy developed earlier, to a tethered flying wing experiment, known as the Caltech-ducted fan. Since the derived CLF is to be used in a receding horizon scheme, we only need the CLF as a stability safeguard, therefore we only consider the single quadratic Lyapunov function case.

5. THE CALTECH-DUCTED FAN

The Caltech-ducted fan is an experimental test bed developed to facilitate the study of uninhabited combat aerial vehicles (UCAVs). These highly manoeuverable aircraft are designed to operate without a pilot on board. The pilot will be in a ground- or airborne-based control room far from the actual vehicle. Using the state-of-the-art virtual reality technology together with proper control schemes should make UCAVs a practical reality. Key advantages in the use of such vehicles include taking pilots out of harm's way and potentially higher performance manoeuvering.

In this section, we apply receding horizon techniques to hover and forward flight models of the Caltech-ducted fan experiment.

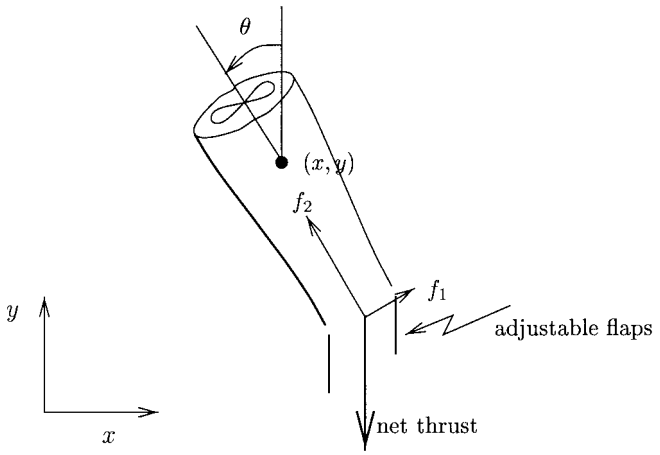

Figure 1. Schematics of the planar-ducted fan.

5.1. *Ducted fan at hover*

The dynamics of the Caltech-ducted fan are representative of a vertical take-off and landing (VTOL) aircraft such as Harrier in hover mode or a thrust vectored aircraft such as F18-HARV or X-31 in forward flight [19,20]. This system has been used in a number of studies and papers and continues to evolve. For instance, comparison of several linear and nonlinear controllers was performed in References [21–23]. In this section, we describe a simple planar model of the fan shown in Figure 1. This model has been used for hover control design for the actual experiment. More recently, the authors in Reference [24] have successfully used this model to obtain a CLF using state-dependent Ricatti equation methods. The CLF is then used as a terminal cost in the receding horizon scheme.

Let (x, y, θ) denote the position and orientation of the centre of mass of the fan. We assume that the forces acting on the fan consist of a force f_1 perpendicular to the axis of the fan acting at a distance r and a force f_2 parallel to the axis of the fan. Denoting m, J, and g as the mass of the fan, the moment of inertia, and the gravitational constant, respectively, the equations of motion can be written as follows [19]:

$$\begin{aligned} m\ddot{x} &= -d\dot{x} + f_1 \cos\theta - f_2 \sin\theta \\ m\ddot{y} &= -d\dot{y} + f_1 \sin\theta + f_2 \cos\theta - mg \\ J\ddot{\theta} &= rf_1 \end{aligned} \tag{6}$$

where the drag terms are modelled as viscous friction with d being the friction coefficient. The numerical data for the experiment are as follows: $m = 11.2$ kg, $g = 0.28$ m/s^2, $J = 0.0462$ kg m^2, $r = 0.156$ m, $d = 0.1$ Ns/m. Note that, due to the use of a counterweight for balancing the fan, the gravitational constant is not 9.8 m/s^2. It is convenient to redefine the inputs so that the origin is an equilibrium point of the system with zero input. Letting $u_1 = f_1$ and $u_2 = f_2 - mg$, the equations of motion can be written as follows:

$$m\ddot{x} = -mg \sin\theta - d\dot{x} + u_1 \cos\theta - u_2 \sin\theta$$

$$m\ddot{y} = mg(\cos\theta - 1) - d\dot{y} + u_1 \sin\theta + u_2 \cos\theta$$

$$J\ddot{\theta} = ru_1 \tag{7}$$

These equations are referred to as the *planar-ducted fan equations*. The following quadratic performance index was used in the quasi-LPV scheme:

$$\mathscr{J} = \int_0^\infty (\bar{x}^{\mathrm{T}}(\tau)Q\bar{x}(\tau) + u^{\mathrm{T}}(\tau)Ru(\tau))\,\mathrm{d}\tau$$

where $\bar{x} = [x \;\; \dot{x} \;\; y \;\; \dot{y} \;\; \theta \;\; \dot{\theta}]^{\mathrm{T}}$ and R and Q are diagonal matrices given by

$$Q = \mathrm{diag}([\,0.5 \quad 1 \quad 5 \quad 1 \quad 5 \quad 1\,]) \tag{8}$$

$$R = \mathrm{diag}([\,2 \quad 1\,]) \tag{9}$$

To obtain a CLF for the planar-ducted fan using a quasi-LPV strategy, we must choose a set of varying parameters. For the planar-ducted fan, $\rho = \theta$ is chosen to be the only varying parameter with range $\mathscr{P} = [-\pi/2, \pi/2]$. As a first attempt, we tried to find a quadratic CLF so that no *a priori* bound on parameter variation would be needed. Unfortunately, the resulting convex programme (for the desired large operating region) is not feasible. Therefore, we switched to searching for a parameter-dependent Lyapunov function with θ as the varying parameter. The bound on the rate variation on θ was chosen to be 10, i.e. $|\theta| \leqslant 10$.

The nonlinear system vector fields f and g can be put into a quasi-LPV form by choosing $A(\theta)$ and $B(\theta)$ according to [25,26]:

$$A(\theta) = \begin{bmatrix} 0 & 1 & 0 & 0 & 0 & 0 \\ 0 & -\dfrac{d}{m} & 0 & 0 & -\dfrac{g\sin\theta}{\theta} & 0 \\ 0 & 0 & 0 & 1 & 0 & 0 \\ 0 & 0 & 0 & -\dfrac{d}{m} & \dfrac{g(\cos\theta - 1)}{\theta} & 0 \\ 0 & 0 & 0 & 0 & 0 & 1 \\ 0 & 0 & 0 & 0 & 0 & 0 \end{bmatrix}$$

$$B(\theta) = \begin{bmatrix} 0 & 0 \\ \dfrac{\cos\theta}{m} & -\dfrac{\sin\theta}{m} \\ 0 & 0 \\ \dfrac{\sin\theta}{m} & \dfrac{\cos\theta}{m} \\ 0 & 0 \\ \frac{r}{j} & 0 \end{bmatrix} \tag{10}$$

To enable the use of LMI techniques, a finite affine parametrization of the inverse Lyapunov matrix $X(\rho)$ was used. In particular, using symmetric matrices X_i, $i = 1, \ldots, 5$, as LMI variables,

$X(\rho)$ is given by

$$X(\rho) = \sum_{i=1}^{5} c_i(\rho) X_i$$

where the functions $c_i(\rho)$ are the fifth order Legendre polynomials on $\mathscr{P}$,

$$\{c_i(\rho)\} = \left\{ 1, \frac{2}{\pi}\theta, \left(3\left(\frac{2}{\pi}\theta\right)^2 - 1\right) \Big/ 2, \left(5\left(\frac{2}{\pi}\theta\right)^3 - 3\left(\frac{2}{\pi}\theta\right)\right) \Big/ 2 \right.$$
$$\left. \left(35\left(\frac{2}{\pi}\theta\right)^4 - 30\left(\frac{2}{\pi}\theta\right)^2 + 3\right) \Big/ 8 \right\}$$

The orthogonality of the set $\{c_I(\rho)\}$ over $\mathscr{P}$ appears to have beneficial numerical properties in the LMI computations.

Once a CLF is obtained, it can be used as a terminal cost in a receding horizon optimization. Also, when the horizon length is long enough, the local CLF obtained by solving an LQR problem for the linearized dynamics may also be used. In the next section, we discuss some simulation results for the planar-ducted fan model, using CLFs from LQR and LPV as a terminal cost in the receding horizon scheme.

5.1.1. Simulation results

We present receding horizon simulations for the various terminal costs over different horizon lengths for the initial condition

$$[x \quad \dot{x} \quad y \quad \dot{y} \quad \theta \quad \dot{\theta}](0) = [-1 \quad 2.5 \quad 0 \quad 0 \quad -45^\circ \quad 0]$$

The baseline infinite horizon cost (with corresponding trajectory) was (approximately) calculated by solving a finite horizon optimization problem with LQR terminal cost with a sufficiently long horizon (known to converge to the infinite horizon case).

It can be seen from the simulation plots that a simple LQR controller does not stabilize the system from the given initial condition, whereas the LPV controller does. This is not surprising since the LPV controller is designed with much more information about the system nonlinearities.

Receding horizon control can be viewed as a compromise between a CLF controller (obtained as a zero horizon optimal controller) and the infinite horizon optimal controller. That is, we expect the short horizon controller to have a behaviour similar to that obtained by minimizing $(\dot{V} + q)(x, u)$ and progressing to the desirable properties of the infinite horizon controller as the horizon length is increased. It is thus not a surprise that the receding horizon controller using the simple quadratic CLF from LQR is ineffective (i.e. unstable) for small horizon lengths.

Figure 2 depicts the x–y components of the finite horizon optimal trajectories with linear quadratic terminal cost for horizon lengths of 0.05, 0.1, 0.15, and 0.2 s. As noted in the figure, the terminal point is far from the origin. This contributes to the lack of stability of the resulting receding horizon controller from the given initial condition. For sufficiently long enough horizons, however, the finite horizon optimal trajectories do approach the origin and the resulting receding horizon controllers stabilize the system, as shown in Figure 3. This is due to the fact that the set Ω_{r_v}, defined in Section 2, can be reached from the initial condition at the end

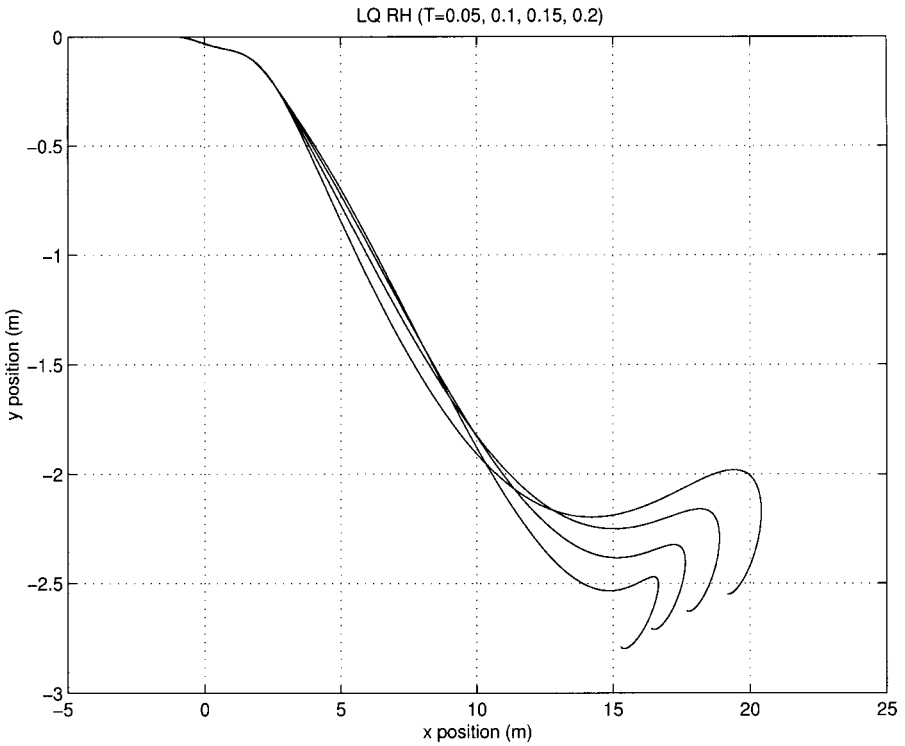

Figure 2. x–y position of the fan for four one shot trajectories with different horizon lengths, from 0.05 to 0.2 s. The resulting receding horizon controller does not stabilize the system from the chosen initial condition.

of the horizon, as the horizon length is increased. Note that the trajectories also converge to the optimal one as T approaches infinity (see Figure 3).

The x–y trajectories for several receding horizon iterations with different horizon lengths with CLF from LPV is depicted in Figure 4. The initial condition chosen was the same as in (11). Note the difference in the orientation of the fan in the case of LQR and LPV terminal costs. Also, note that the CLF from LPV is stabilizing with a 0 horizon length which corresponds to no on-line computation at all, i.e. applying the LPV controller.

One might think that since stability is guaranteed by having a CLF as terminal cost, any positive definite function lower bounded by the CLF would also be a legitimate choice. Simulation results indicate that this is not the case, and merely putting a quadratic penalty which is greater than the value of the CLF (and therefore an upper bound on the cost-to-go) is not sufficient. Figure 5 depicts the simulation results for the receding horizon scheme with having a penalty of the form of $\gamma\|x(t+T)\|^2$ where $\gamma > 0$ is chosen such that $\gamma\|x\|^2 > V(x)\ \forall x$. Shown in Figure 5 are again x–y trajectories for various choices of T. Note that even for long horizon lengths, the performance is not satisfactory at all.

An interesting comparison between the three discussed choices for the terminal cost is shown in Figure 6. The horizon length is plotted on the horizontal axis, and the ratio of the actual cost

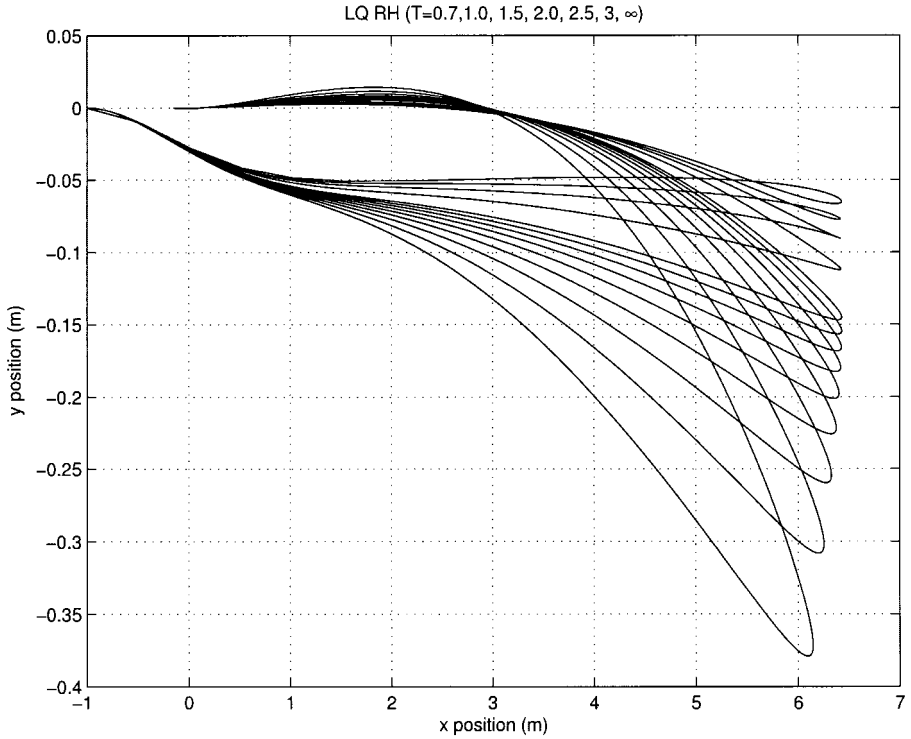

Figure 3. x–y position of the fan for RH with quadratic CLF.

to the optimal cost is plotted on the vertical axis. Note the fast convergence of the cost to the optimal, when the CLF from LQR is chosen as the terminal cost. Interestingly, the choice of CLF from LPV as terminal cost starts at a much lower cost but longer horizon length is needed to converge to the optimal one.

In fact, for horizon lengths of $T \geqslant 0.6$, using the CLF from LQR results in a lower cost due to the fact that the optimal value function is well approximated by the CLF from LQR method, in a suitable neighbourhood of the origin. We can, therefore, conclude that the CLF from LPV methods is suitable when long-optimization horizons are not possible due to costly computation. Finally, having a terminal cost of the form of a quadratic upper bound on the cost-to-go does not work even for very long horizon lengths.

5.2. *Ducted fan in forward flight*

In the previous section, we dealt with a simplified model of the ducted fan around hover. The fan was modelled as a rigid body and the aerodynamic forces were totally ignored. In forward flight, however, one can no longer ignore the aerodynamic forces and moments, since they are the dominant forces that make the ducted fan fly.

An activity to build up aerodynamic models for the ducted fan was established at Caltech [27,28]. However, obtaining steady-state flight data has proved to be much more challenging

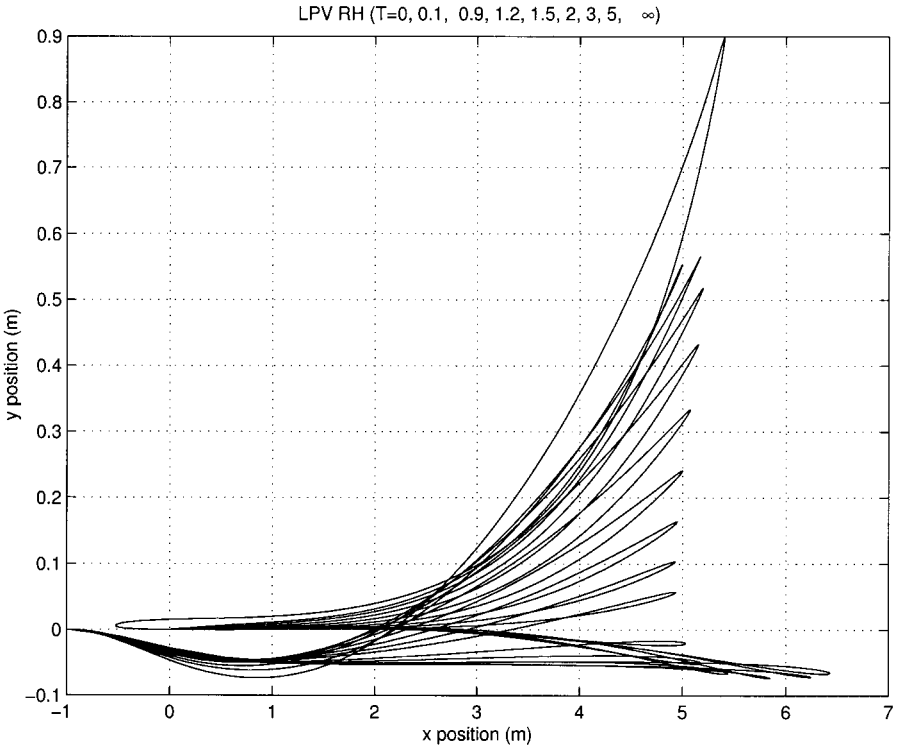

Figure 4. x–y position of the fan for receding horizon with the CLF from LPV.

than expected. This is mainly due to a periodic drag force resulting from the interaction of a wing tip vortex with the walls in the lab (see Figures 7 and 8 for a view of the experimental set-up).

A first step in obtaining suitable models is to familiarize oneself with the flight of this vehicle by doing a significant amount of manual flight. The aggressive capabilities of the system have been explored through *manual* flip and turn around maneuvers [27–29]. Some of these *high angle of attack* manoeuvres are depicted in Figure 9. Angle of attacks of close to 70° are reported in these experiments [28].

In spite of the problems arising from the periodic drag force, the results look quite promising, especially for the purpose of obtaining a model that captures the *essential features* of the system.

After getting a general picture of the capabilities of the system, an important step in modelling is to obtain the experimental *equilibrium manifold*. The equilibrium manifold is the surface resulting from setting the right-hand side of the equations of motion to zero. Experimentally, points on this surface can be found by performing steady flights at different velocities. Corresponding to each velocity, there is an angle of attack as well as the thrust force and thrust angle that would keep the vehicle in that equilibrium point. Figures 10 and 11 depict the experimental and the model equilibrium manifolds.

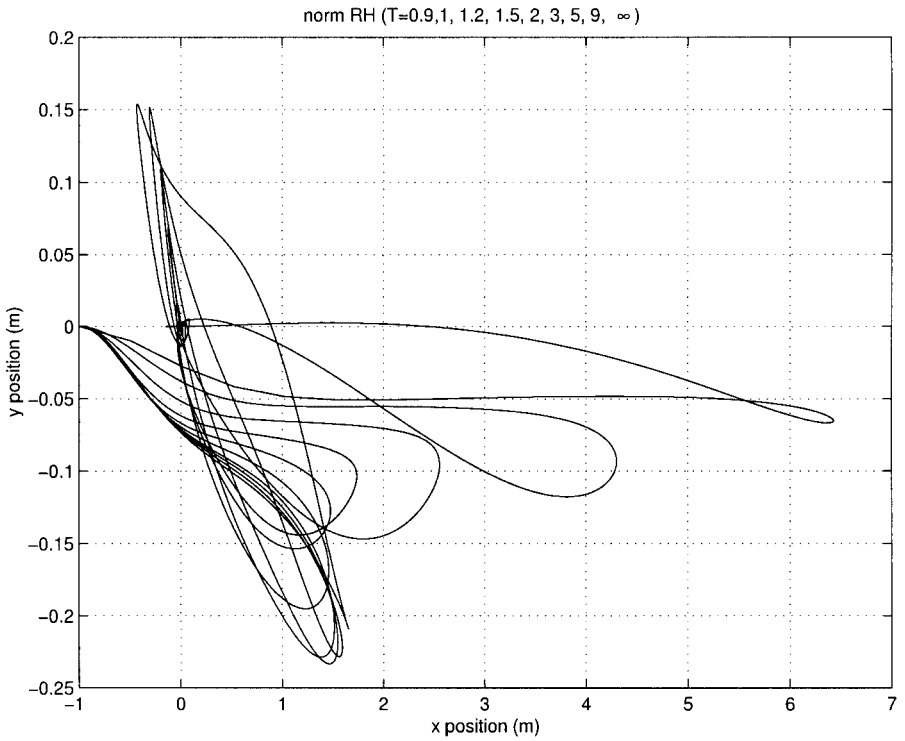

Figure 5. x–y position of the fan for receding horizon with $\gamma\|x\|^2$ as penalty.

5.2.1. Modelling

The ducted fan is modelled as a flying wing with vectored thrust, as in Figure 12. The effect of the newly designed thrust-vectoring nozzle is modelled as a vectored force applied at a fixed position on the flight vehicle. The parameters for this model were estimated using static force/moment measurements. Using the experimental equilibrium manifold, a plausible aerodynamic model was obtained.

The equations of motion for the thrust-vectored flying wing of Figure 12 are as follows:

$$\begin{aligned} m\dot{V} &= -D(V,\alpha) - W\sin\gamma + T\cos(\alpha+\delta_T) \\ mV\dot{\gamma} &= L(V,\alpha) - W\cos\gamma + T\sin(\alpha+\delta_T) \\ \dot{\theta} &= q \\ J\dot{q} &= M(V,\alpha) - Tl_T\sin(\delta_T) \end{aligned} \tag{11}$$

where T is the thrust force, and δ_T is the angle at which thrust is applied. It will be natural to take as state and control variables $x = (V, \gamma, q, \alpha)$, where $\gamma = \theta - \alpha$ is the *flight path angle*, $q = \dot{\theta}$ and $u = (T, \delta_T)$.

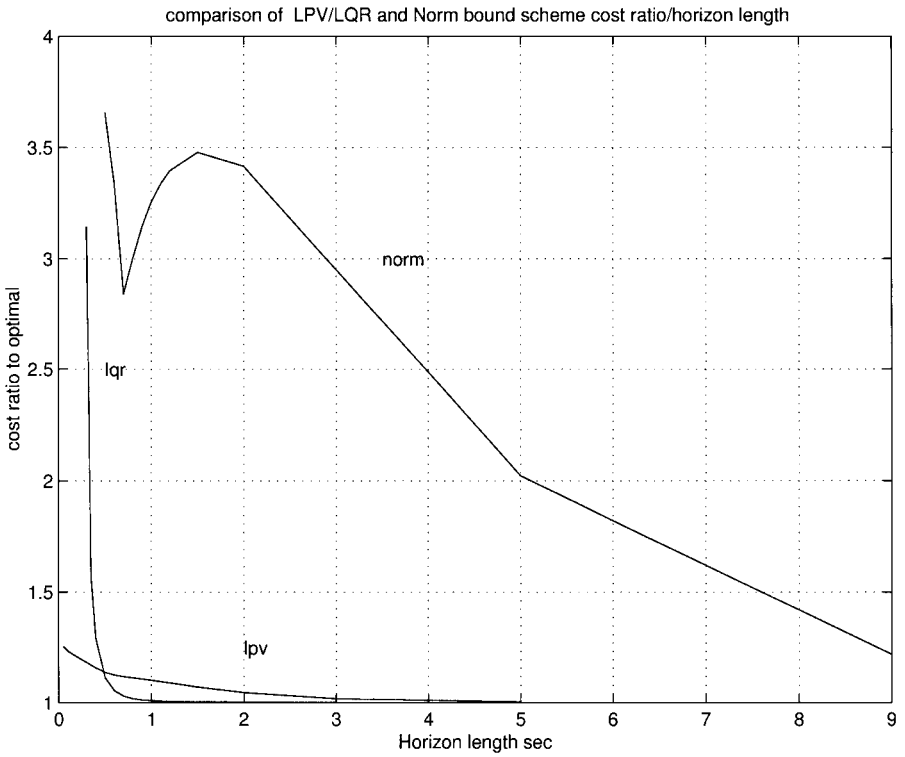

Figure 6. Ratio of the cost to the optimal vs the horizon length.

The physical parameters for this model are $m = 12$ kg, $g = 0.6$ m/s^2, $S = 0.61$ m^2, $\rho = 1.2$ kg/m^3, $l_T = 0.31$ m, $J = 0.24$ kg m^2. The lift, drag and moment terms can be written as follows:

$$L(V,\alpha) = \tfrac{1}{2}\rho V^2 S C_L(\alpha)$$

$$D(V,\alpha) = \tfrac{1}{2}\rho V^2 S C_D(\alpha)$$

$$M(V,\alpha) = \tfrac{1}{2}\rho V^2 S \bar{c} C_M(\alpha) \tag{12}$$

where $\bar{c} = 0.5$ m, and $C_L(\alpha), C_D(\alpha), C_M(\alpha)$ are the lift, drag and moment coefficients, respectively. Using the experimental data from the equilibrium manifold as well as estimates of the thrust and thrust angle given in Figures 10 and 11, one can come up with plausible estimates for the lift, drag and moment coefficients as depicted in Figures 13 and 14.

From the discontinuity in the lift curve, one can notice that stall occurs between 16° and 20° angle of attack. More noticeable is the change in pitching moment at these angle of attacks. Stall can also be noticed from Figure 11 which depicts the thrust angle vs velocity for the equilibrium manifold.

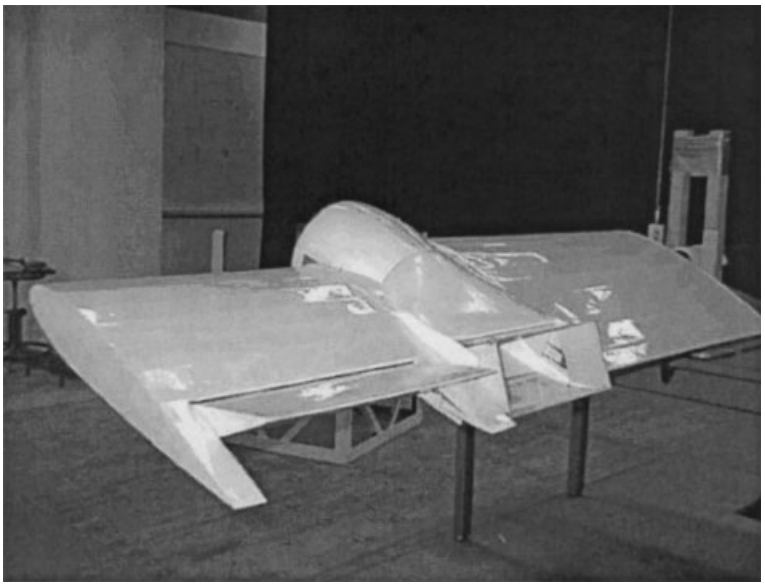

Figure 7. The wing has been redesigned to improve the thrust vectoring.

An interesting point worth mentioning is that one would not see the usual drop in the lift curve after the wing stalls. This is probably due to the fact that the fuselage housing the fan starts to act as a lifting body at these angle of attacks. Worthwhile noting is the fact that the lift, drag, and moment curves fit nicely with the equilibrium manifold data. Locally (i.e. up to stall), lift, drag and moment curves are expressed by the following equations as functions of the angle of attack in radians:

$$C_L(\alpha) = C_{l_\alpha}\alpha = 3.256\alpha$$

$$C_D(\alpha) = C_{d_0} + C_{d_\alpha}\alpha^2 = 0.1716 + 2.395\alpha^2$$

$$C_M(\alpha) = C_{M_\alpha}\alpha = -0.0999\alpha \tag{13}$$

Roughly speaking, the thrust can range from 0 to 13.5 N and can be vectored a little more than 25°, i.e. $\delta_T \leqslant 0.45$ rad.

While the input variables in the model are the thrust force T and the thrust angle δ_T, the control inputs in the experiment are the motor voltage V_m and the commanded paddle angle δ_p. We have the following relationship between the two pair of inputs:

$$\delta_T = 0.684\delta_p$$

$$T = 46.5V_m - 5 \tag{14}$$

Overall, the above model is a plausible description for the Caltech-ducted fan, although much work remains in the understanding of the nature of uncertainties, both external disturbances and model uncertainties.

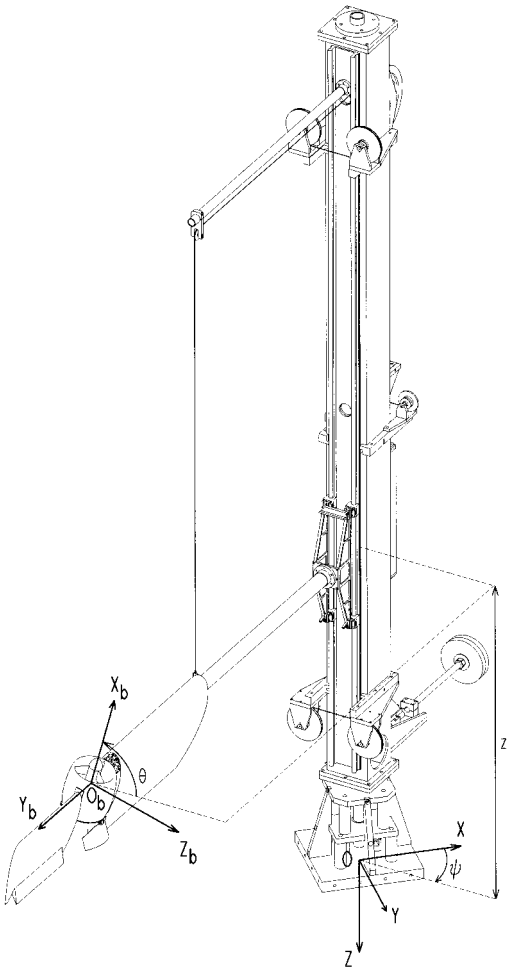

Figure 8. The Caltech-ducted fan [27].

5.2.2. Control of the ducted fan in forward flight

So far, we have discussed a model of the Caltech-ducted fan which is suitable for control purposes.

Following the discussion in Section 4, we now develop a quasi-LPV scheme to generate a CLF suitable for receding horizon control. The objective of the controller is to regulate the ducted fan at a specific point on the equilibrium manifold.

Our objective is to regulate the ducted fan at $V = 6$ m/s. Using Figures 10 and 11, the corresponding angle of attack, thrust, and thrust angle are as follows:

$$\alpha_0 = \theta_0 = 10.149^\circ, \quad T_0 = 3.2005 \text{ N}, \quad \delta_{T_0} = -7.9^\circ$$

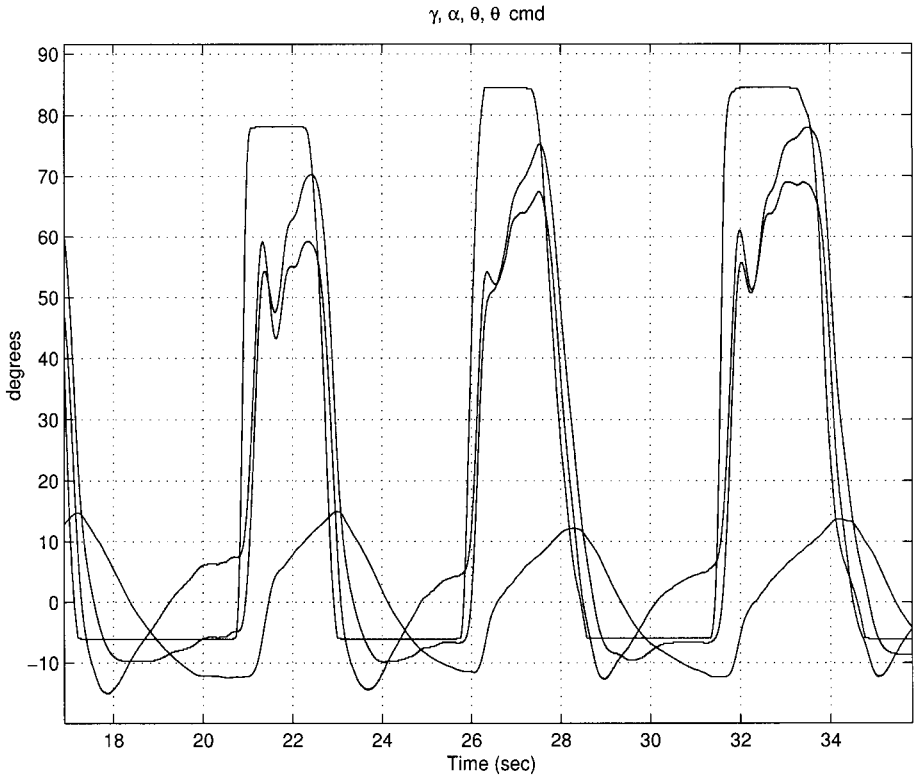

Figure 9. High angle of attack manoeuvering of the Caltech-ducted fan. Shown here are the commanded pitch θ_{cmd}, α, θ and γ.

In order to be able to use the quasi-LPV scheme to generate a CLF, we first have to do a co-ordinate translation so that the desired equilibrium is the origin of the translated system. The next step is to choose a set of varying parameters. Contrary to the planar model where only the pitch angle θ was the varying parameter, we need to choose three terms. We would need two out of the three angles α, θ, γ as well as the velocity V.

For convenience, α, θ, and V are chosen. Note that the new states are $\bar{V} = V - V_0$, $\bar{\alpha} = \alpha - \alpha_0$ and $\bar{\theta} = \theta - \theta_0$. Also, $\bar{q} = q = \dot{\theta}$. As can be seen from (12), the model is not *affine* in control, hence not suitable for use in the LPV scheme. In order to avoid this problem, the following change of variables are made, and forces in the x and z direction are chosen as inputs: $F_x := T\cos(\delta_T)$ $F_z := T\sin(\delta_T)$. We can now describe the equations of motion in the new translated co-ordinates as follows:

$$\dot{\bar{x}} = A(\bar{V}, \bar{\alpha}, \bar{\theta})\bar{x} + B(\bar{V}, \bar{\alpha}, \bar{\theta})\bar{u} \tag{15}$$

where

$$\bar{u} := u - u_0 = \begin{bmatrix} \bar{F}_x \\ \bar{F}_z \end{bmatrix} = \begin{bmatrix} F_x - F_{x_0} \\ F_z - F_{z_0} \end{bmatrix} \tag{16}$$

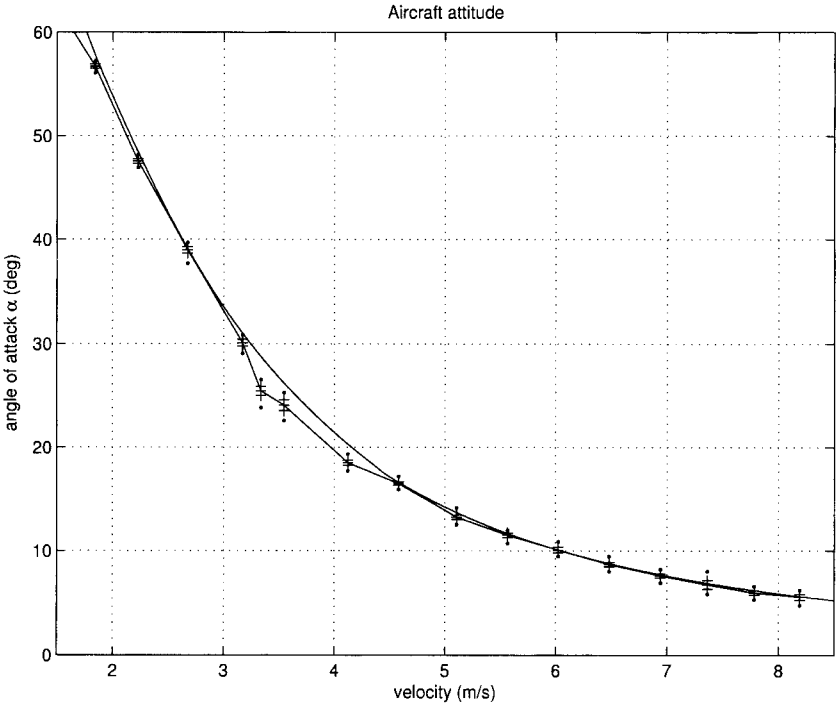

Figure 10. Required angle of attack vs velocity for points on the model and experimental equilibrium manifold. For each flight condition, the average, standard deviation, and the range of values (minimum and maximum) are plotted [28].

and

$$A(\bar{V},\bar{\alpha},\bar{\theta}) := \begin{bmatrix} A_{11} & A_{12} & A_{13} & 0 \\ A_{21} & A_{22} & A_{23} & 1 \\ 0 & 0 & 0 & 1 \\ A_{41} & A_{42} & 0 & 0 \end{bmatrix}, \qquad B(\bar{V},\bar{\alpha},\bar{\theta}) := \begin{bmatrix} \dfrac{\cos(\bar{\alpha}+\alpha_0)}{m} & \dfrac{\sin(\bar{\alpha}+\alpha_0)}{m} \\ -\dfrac{\sin(\bar{\alpha}+\alpha_0)}{m(\bar{V}+V_0)} & \dfrac{\cos(\bar{\alpha}+\alpha_0)}{m(\bar{V}+V_0)} \\ 0 & 0 \\ 0 & \frac{l_T}{J} \end{bmatrix}$$

After a set of rather tedious calculations, the elements of the A matrix can be written as follows:

$$A_{11} = -\frac{1}{2}\frac{\rho S(\bar{V}+2V_0)(C_{d_0}+C_{d_\alpha}(\bar{\alpha}+\alpha_0)^2)}{m}$$

$$A_{12} = -\frac{1}{2}\frac{\rho V_0^2 S C_{d_\alpha}(\bar{\alpha}+2\alpha_0)}{m} + g\sin\left(\frac{\bar{\theta}-\bar{\alpha}}{\pi}\right)\pi(\bar{\theta}-\bar{\alpha})^{-1}$$
$$+ \frac{1}{2}\left(\frac{\cos(\alpha_0+\frac{1}{2}\bar{\alpha})F_{z_0}}{m} - \frac{\sin(\alpha_0+\frac{1}{2}\bar{\alpha})F_{x_0}}{m}\right)\sin\left(\frac{1}{2}\frac{\bar{\alpha}}{\pi}\right)\alpha^{-1}\pi$$

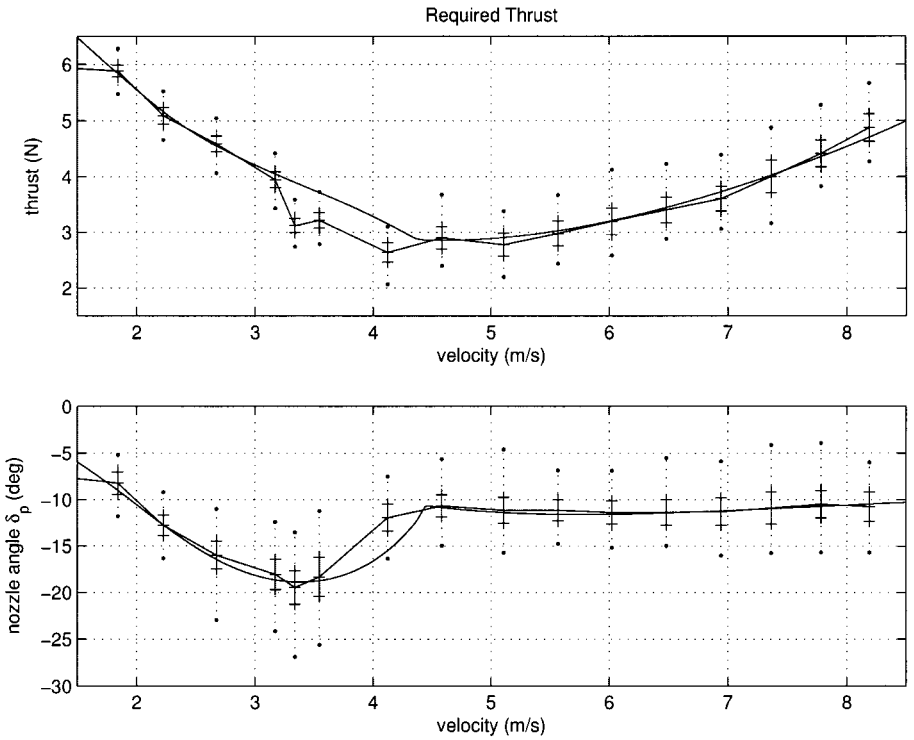

Figure 11. Required thrust T and paddle (nozzle) angle δ_p at different velocities for points on the equilibrium manifold. For each flight condition, the average, standard deviation and the range of values (minimum and maximum) are plotted.

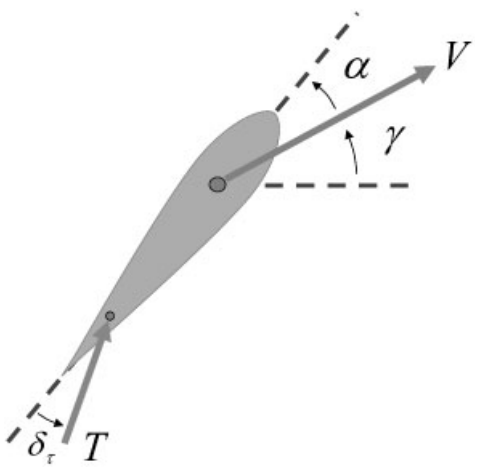

Figure 12. Schematics of the thrust-vectored flying wing.

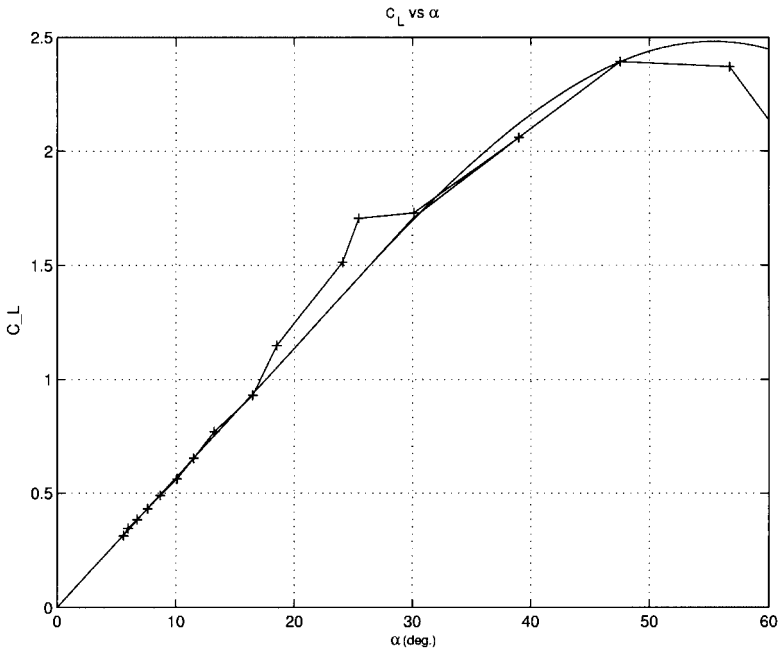

Figure 13. Experimental and model curves for the lift coefficient $C_L(\alpha)$.

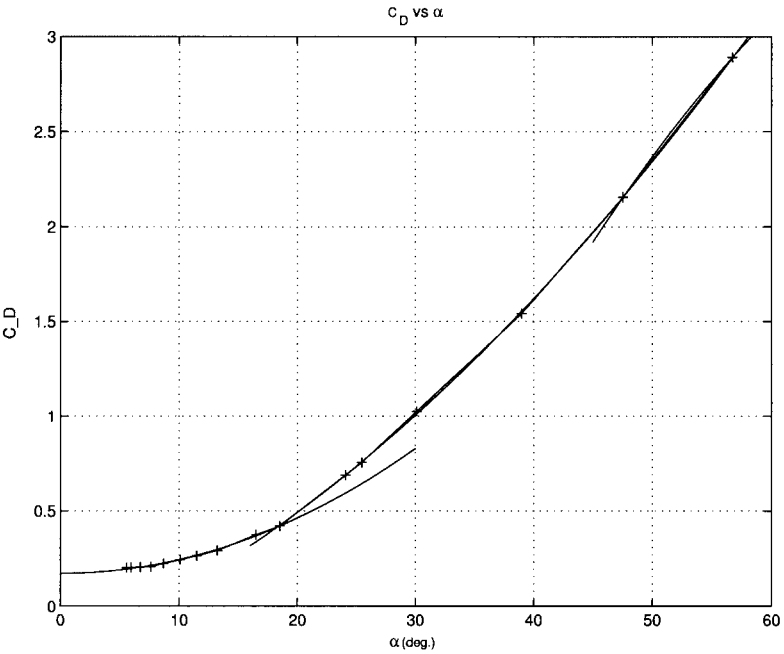

Figure 14. Experimental and model curves for the drag coefficient $C_D(\alpha)$.

$$
\begin{aligned}
A_{13} &= -g \sin\left(\frac{\bar{\theta}-\bar{\alpha}}{\pi}\right)\pi(\bar{\theta}-\bar{\alpha})^{-1} \\
A_{21} &= -\frac{1}{2}\frac{\rho S C_{l_\alpha}(\bar{\alpha}+\alpha_0)}{m} - \frac{g}{V_0(\bar{V}+V_0)} + \frac{F_{x_0}\sin(\alpha_0) - F_{z_0}\cos(\alpha_0)}{mV_0(\bar{V}+V_0)} \\
A_{22} &= -\frac{g(\cos(\bar{\theta}-\bar{\alpha})-1)}{(\bar{\theta}-\bar{\alpha})(\bar{V}+V_0)} - \frac{1}{2}\frac{\rho S C_{l_\alpha} V_0}{m} \\
&\quad - 2\left(\cos\left(\alpha_0+\frac{\bar{\alpha}}{2}\right)F_{x_0} + \sin\left(\alpha_0+\frac{\bar{\alpha}}{2}\right)F_{z_0}\right)\sin\left(\frac{\alpha}{2\pi}\right)\frac{\pi}{\alpha}(m(\bar{V}+V_0))^{-1} \\
A_{23} &= \frac{g(\cos(\bar{\theta}-\bar{\alpha})-1)}{(\bar{\theta}-\bar{\alpha})(\bar{V}+V_0)} \\
A_{41} &= \frac{1}{2}\frac{\rho(\bar{V}+2V_0)S\bar{c}C_{M_\alpha}(\bar{\alpha}+\alpha_0)}{J} \\
A_{42} &= \frac{1}{2}\frac{\rho V_0^2 S\bar{c}C_{M_\alpha}}{J}
\end{aligned}
\tag{17}
$$

Once the equations of motion are represented in the appropriate state-dependent form, the next step is to formulate a suitable performance index to be used in the quasi-LPV scheme.

It is well known that choosing a suitable performance index such that all desired aspects of the problem are taken into account, can be quite difficult. We know that in order to regulate the ducted fan to a point on the equilibrium manifold, the flight path angle must be regulated to 0 therefore, it would be appropriate to put a large weight on the flight path angle in the optimization criterion. Since in our quasi-LPV modelling we did not choose γ as the varying parameter, it would be convenient at this point to choose the flight path angle γ over the pitch angle θ to be a state. Hence, we perform the following change of coordinates:

$$
\begin{bmatrix} V \\ \gamma \\ \alpha \\ q \end{bmatrix} = T_\gamma \begin{bmatrix} V \\ \alpha \\ \theta \\ q \end{bmatrix}, \qquad T_\gamma = \begin{bmatrix} 1 & 0 & 0 & 0 \\ 0 & -1 & 1 & 0 \\ 0 & 1 & 0 & 0 \\ 0 & 0 & 0 & 1 \end{bmatrix} \tag{18}
$$

The new set of coordinates is called the *wind coordinates*. Also, the following Q and R matrices are chosen in conjunction with the quasi-LPV model to generate a CLF.

$$
\begin{aligned}
Q &= \mathrm{diag}[\,50 \quad 4000 \quad 0.01 \quad 10\,] \\
R &= \mathrm{diag}[\,0.5 \quad 4\,]
\end{aligned}
\tag{19}
$$

Several simulations were performed with different values of Q and R, and it turned out that the ones used showed satisfactory performance in the nonlinear simulation.

To use the quasi-LPV scheme discussed in Section 4, we first have to pick a gridding region for the varying parameters (states).

Since our simple aerodynamic model is valid locally, the following region is picked for gridding: $V \in [2, 10]$ (17 points), and $\alpha, \theta \in [-50^\circ, 50^\circ]$ (11 points).

Note that the simulation model [27,28] exceeds this local region in terms of the aerodynamic modelling. For simplicity of the LPV design, we have chosen to use the above limited gridding region for CLF design.

Also, note that since the CLF is merely a stability safeguard to be used as terminal cost in the receding horizon scheme, we would be quite happy with a quadratic CLF, provided the resulting convex optimization problem is feasible. This would greatly reduce the number of LMI constraints in equation (5). It turns out that the optimization problem is indeed feasible, and a quadratic CLF does exist. The resulting CLF is $V(x) = x^{\mathrm{T}}Px$ where

$$P = \begin{bmatrix} 107.6001 & 133.0760 & 16.4710 & 7.6684 \\ 133.0760 & 5194.4631 & 1204.7676 & 245.3851 \\ 16.4710 & 1204.7676 & 577.6781 & 117.0480 \\ 7.6684 & 245.3851 & 117.0480 & 36.3148 \end{bmatrix} \tag{20}$$

The above CLF is then used in a receding horizon scheme with a horizon length of $T = 0.5$ and sampling rate of $\delta = 0.05$ s. Also, to compare the results with 'optimal' trajectories, the horizon length is increased to 3 s.

An important issue is magnitude constraints imposed on the control action. As was mentioned earlier, the thrust can not exceed 13.5N, and can be only vectored for about 25°. This would translate to the following bounds on the actual control actions V_{m} and δ_{p}:

$$\begin{aligned} 0.13\ \mathrm{V} \leqslant V_{\mathrm{m}} \leqslant 0.35\ \mathrm{V} \\ -40^\circ \leqslant \delta_{\mathrm{p}} \leqslant 40^\circ \end{aligned} \tag{21}$$

In order to simulate the system in the forward flight mode, the following initial condition was chosen: $V = 6$ m/s $\gamma = -40^\circ$ $\alpha = 10.2^\circ$ $q = 0$. The above initial condition represents a pull-up manoeuvre. Simulation results are depicted in Figures 15 and 16. Also, Figures 17 and 18 depict the one shot 'optimal' trajectories for the same initial condition and a longer horizon length of 3 s.

A more interesting way of plotting trajectories is to show the actual trajectory of the flying wing in the x–z space instead of showing the time trajectories. These plots are shown in Figures 19 and 20 for the receding horizon and one shot trajectories, respectively. In both figures, the ducted fan is shown as a flying wing, with a red line representing the thrust. These figures indicate that with a horizon of only 0.5 s, we get very close to the optimal solution.

One can also include the z dynamics in the equations of motion by letting $\dot{z} = V \sin\gamma$. Using a similar LPV scheme and by penalizing z with a weight of 20, we obtain a quadratic Lyapunov

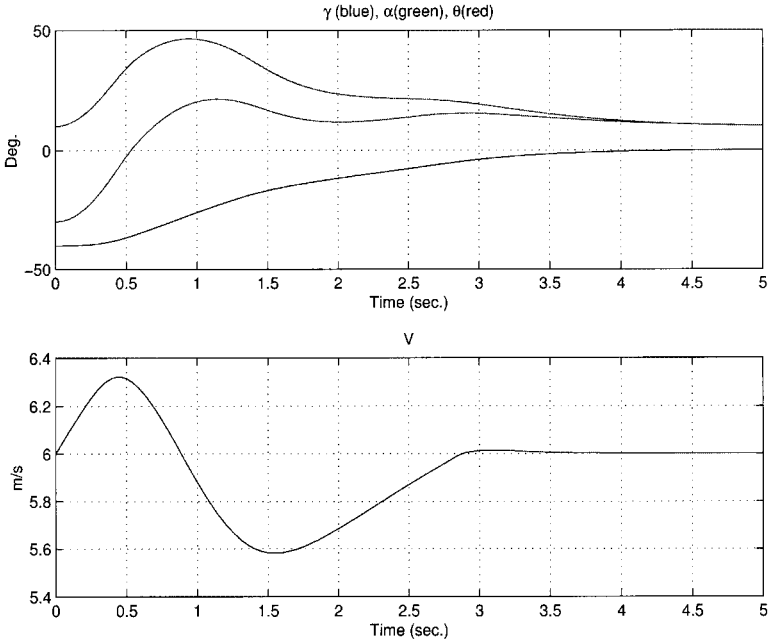

Figure 15. Simulation results for the ducted fan in forward flight with a receding horizon controller $\mathscr{RH}(0.5, 0.05)$. Shown here are the states V, γ, α, θ.

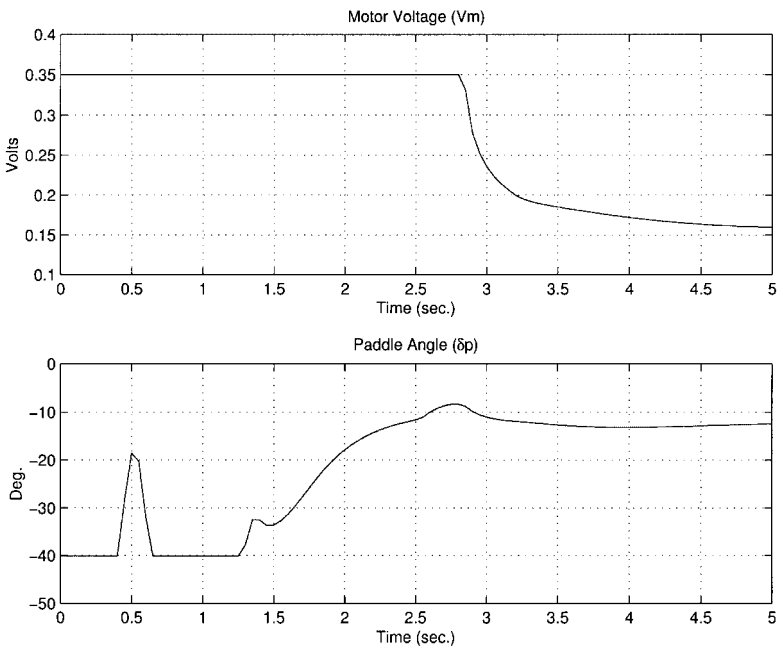

Figure 16. Simulation results for the ducted fan in forward flight with a receding horizon controller $\mathscr{RH}(0.5, 0.05)$. Shown here are the controls V_{m} and δ_{p}.

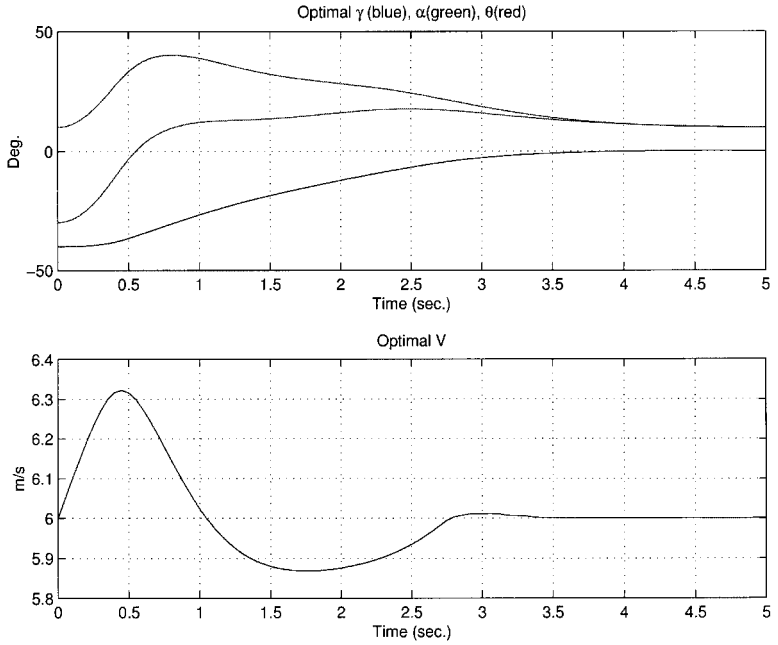

Figure 17. Simulation results for the ducted fan in forward flight with a one shot optimal controller $T = 3$ s. Shown here are the states $V,\ \gamma,\ \alpha,\ \theta$.

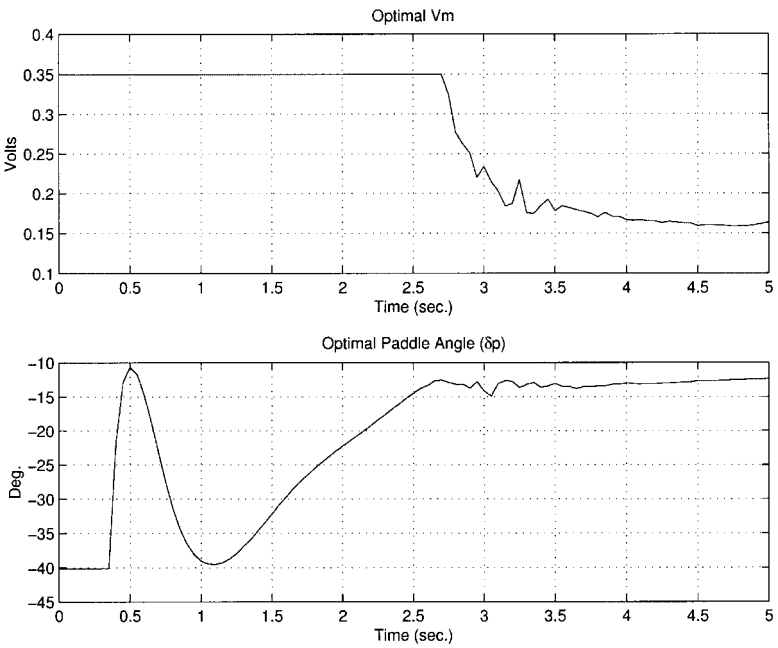

Figure 18. Simulation results for the ducted fan in forward flight with a one shot controller with $T = 3$ s. Shown here are the controls V_{m} and δ_{p}.

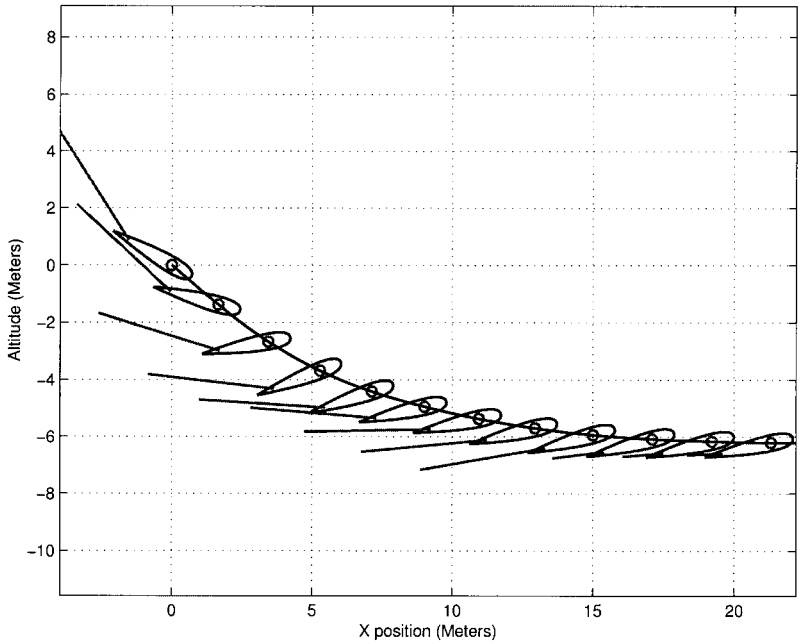

Figure 19. The x–z trajectories for the ducted fan in forward flight with a receding horizon controller $\mathscr{RH}(0.5, 0.05)$. The red lines indicate the thrust, scaled according to the thrust value.

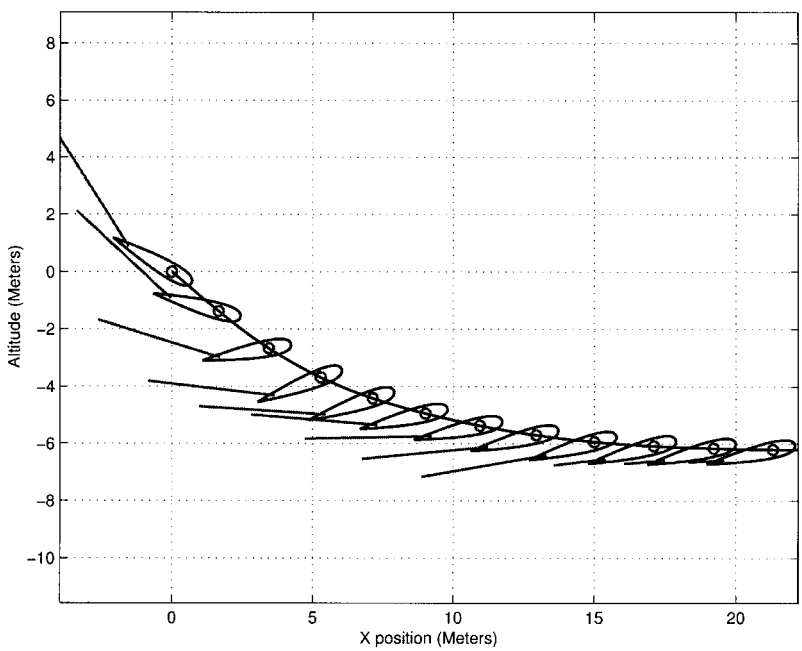

Figure 20. The x–z trajectories for the ducted fan in forward flight with a one shot controller with $T = 3$ s. The red lines indicate the thrust, scaled in length according to the thrust value.

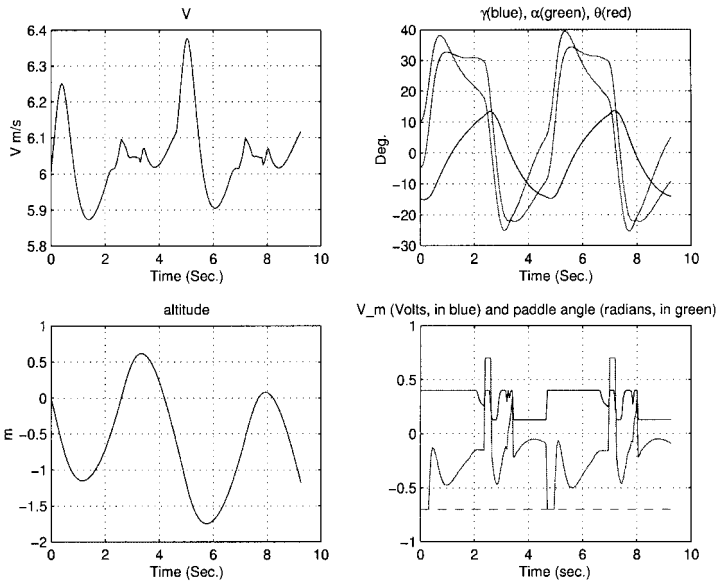

Figure 21. Simulation results for the ducted fan in forward flight with a receding horizon controller $\mathscr{RH}(0.5, 0.05)$. Shown here are the time trajectories for V, γ, α, and θ as well as controls V_m and δ_p. The commanded γ is switched between -15 and 15°.

function $V_z(x) = x^T P_z x$ with P_z given as follows:

$$P_z = \begin{bmatrix} 59.3330 & -1.8051 & -175.5690 & -39.2179 & -5.0851 \\ -1.8051 & 47.6105 & 11.1567 & -3.5507 & -0.6610 \\ -175.5690 & 11.1567 & 854.3814 & 176.9442 & 27.1237 \\ -39.2179 & -3.5507 & 176.9442 & 59.6604 & 7.3196 \\ -5.0851 & -0.6610 & 27.1237 & 7.3196 & 2.0231 \end{bmatrix} \tag{22}$$

Figures 21 and 22 depict the simulation results when the desired flight path angle γ is a square wave, switching between -15 and 15°. Figure 21 depicts the time trajectories of the states and controls, whereas Figure 22 shows the trajectory in the x–z space. As can be seen from both figures, the controls are saturated most of the time. Again, it should be noted that the simulation model extends the local range and includes the stall information. Also, the objective function in the receding horizon optimizations was the same as in the quasi-LPV scheme.

The resulting receding horizon optimizations were performed using RIOTS [30] in the Matlab environment. Each receding horizon iteration (for a 0.5 s horizon length) took about 0.6 s on a Sun Ultra 30 machine. The next step is to verify the simulation results on the actual experiment using a much more efficient optimal trajectory solver recently developed at Caltech [31].

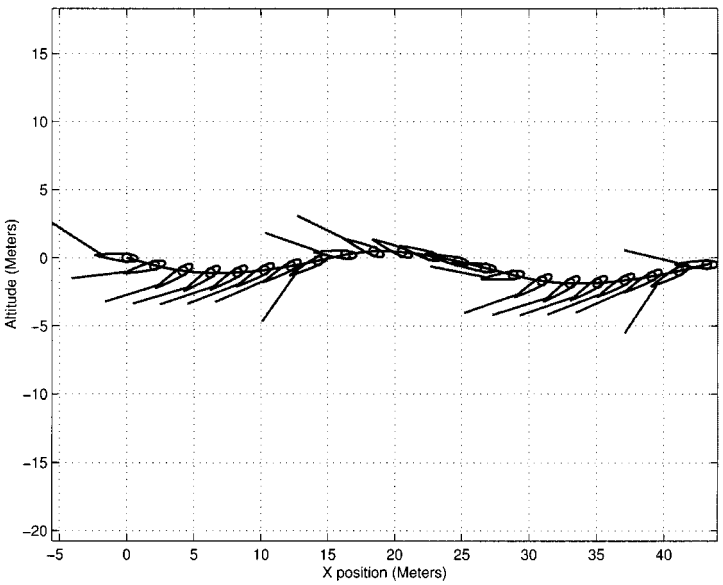

Figure 22. Simulation results for the ducted fan in forward flight with a receding horizon controller $\mathscr{RH}(0.5, 0.05)$. Shown here is the phase trajectory in the x–z plane. The flying wing represents the ducted fan and the red line depicts the thrust, scaled in length according to the actual thrust value. The commanded γ is switched between -15 and 15°.

6. CONCLUSION

The purpose of this paper was to demonstrate the use of a stabilizing receding horizon control methodology on two distinct models of the Caltech-ducted fan experiment. Equations of motion were obtained for the hover mode as well as the forward flight mode. Using quasi-LPV methods discussed in Section 4, several CLFs were obtained and used as terminal cost in the receding horizon scheme. Simulation results suggest that the proposed receding horizon scheme is suitable for regulation of the Caltech-ducted fan and guaranteeing closed-loop stability.

ACKNOWLEDGEMENTS

Research supported in part by AFOSR and DARPA. This research was performed when both authors were at CDS Department, Caltech.

REFERENCES

1. Mayne DQ, Rawlings JB, Rao CV, Scokaert POM. Constrained model predictive control: stability and optimality. *Automatica* 2000; **36**(6):789–814.
2. Keerthi S, Gilbert E. Optimal infinite-horizon feedback laws for a general class of constrained discrete-time systems: stability and moving-horizon approximations. *Journal of Optimization Theory and Applications* 1988; **57**:265–293.
3. Magni L, Sepulchre R. Stability margins of nonlinear receding horizon control via inverse optimality. *Systems and Control Letters* 1997; **32**:241–245.
4. Michalska H, Mayne DQ. Robust receding horizon control of constrained nonlinear systems. *IEEE Transactions on Automatic Control* 1993; **38**(11):1623–1633.

5. De Nicolao G, Magni L, Scattolini R. Stabilizing receding-horizon control of nonlinear time-varying systems. *IEEE Transactions on Automatic Control* 1998; **43**(7):1030–1036.
6. Parisini T, Zoppoli R. A receding horizon regulator for nonlinear systems and a neural approximation. *Automatica* 1995; **31**:1443–1451.
7. Chen H, Allgöwer F. A quasi-infinite horizon nonlinear model predictive control scheme with guaranteed stability. *Automatica* 1998; **34**:1205–1217.
8. Primbs JA, Nevistić V, Doyle JC. A receding horizon generalization of pointwise min-norm controllers. *IEEE Transactions on Automatic Control* 2000; **45**:898–909.
9. Jadbabaie A, Yu J, Hauser J. Unconstrained receding horizon control of nonlinear systems. *IEEE Transactions on Automatic Control* 2001; **46**(5):776–783.
10. Jadbabaie A, Yu J, Hauser J. Unconstrained receding horizon control of nonlinear systems. In *IEEE Conference on Decision and Control*, Phoenix, Arizona 1999; 3376–3381.
11. Jadbabaie A, Hauser J. Relaxing the optimality condition in receding horizon control. In *IEEE Conference on Decision and Control*, 2000.
12. Bardi M, Capuzzo-Dolcetta I. *Optimal Control and Viscosity Solutions of Hamilton–Jacobi–Bellman Equations*. Birkhauser: Boston, 1997.
13. Shamma J, Athans M. Guaranteed properties of gain scheduled control for linear parameter-varying plants. *Automatica* 1991; 559–564.
14. Wu F, Yang HX, Packard A, Becker G. Induced L_2-Norm control for LPV systems with bounded parameter variation. *International Journal of Robust and Nonlinear Control* 1996; **6**:983–998.
15. Huang Y, Jadbabaie A. Nonlinear H_∞ control: an enhanced quasi-LPV approach. In *Proceedings of the IFAC World Congress*, Beijing, China, vol. F, 1999; 85–90.
16. Huang Y. Nonlinear optimal control: an enhanced quasi-LPV approach. *PhD Thesis*, California Institute of Technology, Pasadena, CA, 1998.
17. Cloutier JR, D'Souza CN, Mracek CP. Nonlinear regulation and nonlinear H_∞ control via the state-dependent Riccati equation technique. In *Proceedings of the 1st International Conference on Nonlinear Problems in Aviation and Aerospace*, Daytona Beach, FL, 1996.
18. Balas G, Fialho I, Lee L, Nalabantoglu V, Packard A, Tan W, Wemhoff E, Wolodkin G, Wu F. Theory and applicati6n of linear parameter varying control techniques. *Tutorial Presented at the 1997 Automatic Control Conference*, Albuquerque, NM, 1997.
19. Hauser J, Sastry S, Meyer G. Nonlinear control design for slightly nonminimum phase systems—application to V/STOL aircraft. *Automatica* 1992; **28**:665–679.
20. Murray RM. Modeling of the Caltech ducted fan, class notes for cds 111. *Technical Report*, California Institute of Technology, Control and Dynamical Systems 107–81, 1998.
21. Kantner M, Bodenheimer B, Bendotti P, Murray RM. An experimental comparison of controllers for a vectored thrust ducted fan engine. In *American Control Conference*, Seattle, WA 1995; 1956–1961.
22. Bodenheimer B, Bendotti P, Kantner M. Linear parameter-varying control of a ducted fan engine. *International Journal of Robust and Nonlinear Control* 1996; **6**:1023–1044.
23. van Nieuwstadt M, Murray RM. Real time trejectory generation for differentially flat systems. In *Proceedings of the 1996 IFAC World Congress*, San Franciso, CA 1996.
24. Sznaier M, Cloutier J, Hull R, Jacques D, Mracek C. Receding horizon control Lyapunov function approach to suboptimal regulation of nonlinear systems. *Journal of Guidance, Control, and Dynamics* 2000; **23**(3):399–405.
25. Jadbabaie A, Yu J, Hauser J. Receding horizon control of the Caltech ducted fan: a control Lyapunov function approach. In *IEEE Conference on Control Applications*, Big Island, HI 1999; 51–56.
26. Yu J, Jadbabaie A, Primbs J, Huang Y. Comparison of nonlinear control designs for a ducted fan model. In *Proceedings of the IFAC World Congress*, vol. E, Beijing, China, 1999; 53–58.
27. Milam M, Murray RM. A testbed for nonlinear flight control techniques: the Caltech ducted fan. In *IEEE Conference on Control Applications*, Big Island, HI, 1999; 345–351.
28. Hauser J, Jadbabaie A. Aggressive manoeuvering of a thrust vectored flying wing: a receding horizon approach. In *IEEE Conference on Decision and Control*, Sydney, Australia, 2000.
29. Trotoux M. *Personal communications*, 2000.
30. Schwartz A. Theory and implementation of numerical methods based on Runge–Kutta integration for optimal control problems. *PhD Dissertation*, University of California, Berkeley, 1996.
31. Milam M, Mushambi K, Murray RM. A computational approach to real-time trajectory generation for constrained mechanical systems. In *IEEE Conference on Decision and Control*, Sydney, Australia 2000.

